molecules

MDPI

Article

Vacancy-Induced Magnetism in Fluorographene: The Effect of Midgap State

Daozhi Li [1], Xiaoyang Ma [1,*], Hongwei Chu [1], Ying Li [2], Shengzhi Zhao [1] and Dechun Li [1,*]

[1] School of Information Science and Engineering, Shandong University, Qingdao 266237, China; 201912459@mail.sdu.edu.cn (D.L.); hongwei.chu@sdu.edu.cn (H.C.); Shengzhi_zhao@sdu.edu.cn (S.Z.)
[2] Key Laboratory of Colloid and Interface Chemistry of Education Ministry, School of Chemistry and Chemical Engineering, Shandong University, Jinan 250100, China; yingli@sdu.edu.cn
* Correspondence: mxyacademic@sdu.edu.cn (X.M.); dechun@sdu.edu.cn (D.L.)

Abstract: Based on density functional theory, we have systematically investigated the geometric, magnetic, and electronic properties of fluorographene with three types of vacancy defects. With uneven sublattice, the partial defect structures are significantly spin-polarized and present midgap electronic states. The magnetic moment is mainly contributed by the adjacent C atoms of vacancy defects. Furthermore, the strain dependence of the bandgap is analyzed and shows a linear trend with applied strain. This defect-induced tunable narrow bandgap material has great potential in electronic devices and spintronics applications.

Keywords: fluorographene; vacancy; magnetic moment; strain

Citation: Li, D.; Ma, X.; Chu, H.; Li, Y.; Zhao, S.; Li, D. Vacancy-Induced Magnetism in Fluorographene: The Effect of Midgap State. *Molecules* **2021**, *26*, 6666. https://doi.org/10.3390/molecules26216666

Academic Editors: Kejian Yang and Yuanfu Chen

Received: 16 September 2021
Accepted: 2 November 2021
Published: 3 November 2021

1. Introduction

Graphene has received widespread attention for its unique chemical or physical characteristics and exhibiting great potentials in optics, spintronics, and optoelectronics since its discovery [1–7]. However, the gapless band structure, which fails to switch current "on" and "off", obstructs its applications in electronics such as field-effect transistors (FET). In order to overcome this obstruction, to date, diverse strategies have been proposed to open the zero bandgap and one of the effective schemes is chemical functionalization [8–13]. Functional graphene, including graphene oxide and halogenated graphene, has been proved to possess extraordinary properties as well as an expected tunable bandgap [14–19]. For example, by halogen (F, Cl, Br, I) doping, halogenated graphene is suggested to be capable to regulate the bandgap in a wide range and also could enhance the reaction kinetics of the Li–S cathode, leading to a high-performance lithium battery [20,21]. As the F atom possesses a higher electronegativity than other halogen atoms, fluorinated graphene (CF_x), a typical type of halogenated graphene, has been verified to be more stable than other types, and its properties are strongly dependent on the degree of fluorination [22–24]. By modulating F/C ratios, graphene, a nonmagnetic semimetal, can be transformed into a nonmagnetic/magnetic semiconductor/insulator [25]. With an F atom attached to each C atom, fluorographene (fully fluorinated graphene) was reported to be a high-quality insulator (resistance >10 GΩ at room-temperature) with a wide optical bandgap (3.8 eV), large negative magnetic resistance (a factor of 40 in 9T field), and remarkable mechanical strength, showing great potential in the electronic applications [26,27].

During the past two decades, many efforts have been made to fabricate fluorographene [27–30]. In 2010, Cheng, et al. reported the synthesis of graphene fluoride by reacting graphite and fluorine gas. They demonstrated that the band structure and conductivity of CF_x were reversible by fluorination or reduction reactions [27]. After that, in 2011, Jeon and his collaborators produced fluorographene with the treatment of graphene with xenon difluoride (XeF_2) and pave the way to develop graphene-based semiconductors

by the direct chemical fluorination method [28]. Recently, the successful thermal exfoliation of fluorinated graphene at room temperature indicated the feasibility of producing large-scale fluorographene [30]. However, considering the high temperature involved in the fluorination processes, structural defects, especially vacancy defects may appear and deteriorate the performance of structures such as magnetic momentum and conductivity, which has an important impact on the magnetic and electronic applications [27,31]. Many calculations also show that defects will have a great influence on electromagnetic properties of two-dimensional materials [32,33]. Therefore, it is of great meaning to explore the theoretical mechanism of vacancy defects and deeply understand the defects' influence on structural performance. In this article, we studied fluorographene with three types of vacancy defects, including single F atom vacancy (V_F-fluorographene), single C–F vacancy (V_{sCF}-fluorographene), and double CF vacancy (V_{dCF}-fluorographene) via first-principle theory. The ab initio molecular dynamics (MD) simulations were performed to estimate the thermodynamical stability. The spin-charge density was analyzed to figure out how magnetic moment induced by vacancy defects. Furthermore, band structures, as well as the density of states, are also investigated. Although fluorographene is an insulator with a large bandgap, it can be transformed into a semiconductor by introducing appropriate vacancy defects and the bandgap can be tuned by the external strains.

2. Results and Discussion

To avoid the interactions between defects, 5 × 3 supercell of fluorographene is established. We chose three typical vacancy structures (single F, single C–F, and double C–F vacancy) by referring to the vacancy defect structures in other functional graphene [14,15]. Figure 1 displays the structures of V_F-, V_{CF}- and V_{dCF}-fluorographene, respectively.

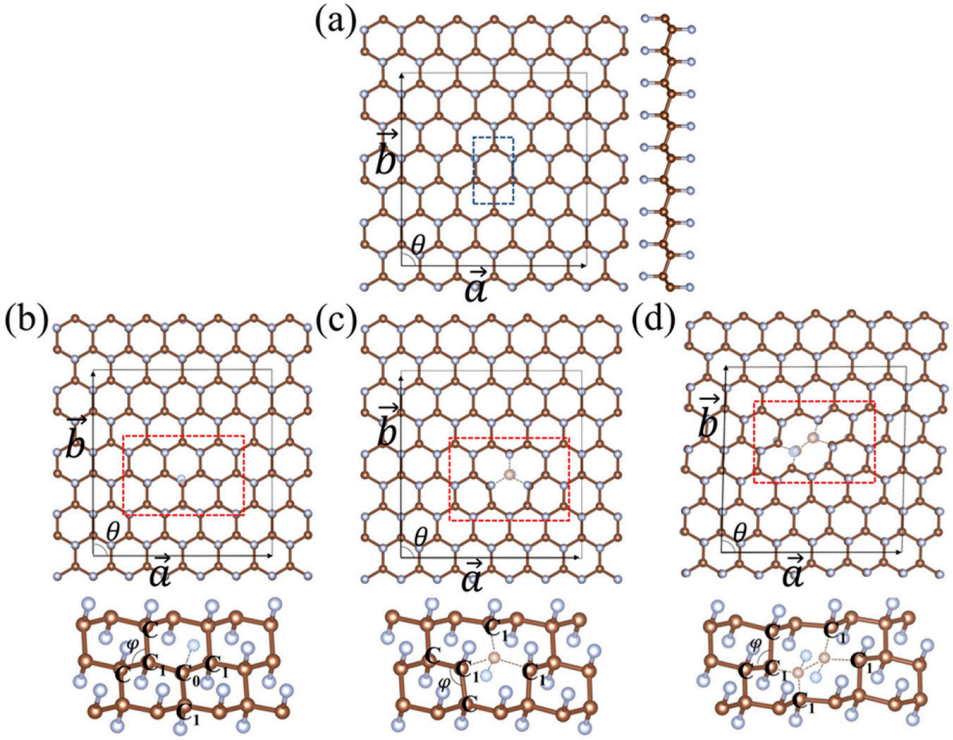

Figure 1. The 5 × 3 supercell of (**a**) fluorographene, and three types of vacancy defects: (**b**) fluorographene with F vacancy (V_F-fluorographene), (**c**) fluorographene with single C–F vacancy (V_{sCF}-fluorographene), and (**d**) fluorographene with double C–F vacancy (V_{dCF}-fluorographene). The brown and light-grey spheres represent C and F atoms, respectively. The blue rectangular in (**a**) is the unit cell of fluorographene, while the red rectangular in (**b**–**d**) represent the areas greatly impacted by vacancy defects.

The C–F bond length (1.384 Å) and angle between adjacent C–C bonds (110.8°) are in good agreement with the previous calculation (1.37 Å/111°) [34]. With an F absence, the C_0 atom in V_F-fluorographene connects to three nearest neighbor C_1 atoms, and there is a slight distortion in the lattice, especially in the red rectangular where the lattice is greatly perturbed by the vacancy defect. The buckling height of the C_0 atom decreases remarkably due to the enhancement of the C_0–C_1 bonding strength. Similarly, for the V_{sCF}- and V_{dCF}-fluorographene, the bond strength of C_1–C enhanced since C_1 atoms move close to their adjacent C atoms. The vacancy defects break the original symmetry of fluorographene. V_F- and V_{sCF}-fluorographene fluorographene shows mirror symmetry, while V_{dCF}-fluorographene shows central symmetry.

The structural data of fluorographene and fluorographene with vacancy defects are summarized in Table 1. The decrease of the average bond length d_{C_1-C} in all these structures confirms the enhancement of C_1–C bonding strength. With the F defect, the average C_1–F bond length d_{C_1-F} in V_F-fluorographene show an unexpected increase, which is quite different from V_{sCF}- and V_{dCF}-fluorographene. This shows that compared to fluorographene, the interaction between C_1 and F atoms of V_F-fluorographene is weaker, while that of V_{sCF}- and V_{dCF}-fluorographene are stronger. The deviation of lattice angle θ in V_{dCF}-fluorographene demonstrates that the deformation caused by the double C–F vacancy is stronger than others.

Table 1. The structural data including lattice information, average bond length (d_{C_1-C} and d_{C_1-F}), average angle between adjacent C_1–C (φ_{C-C_1-C}) and formation energy of fluorographene, V_F-, V_{sCF}-, and V_{dCF}-fluorographene. C_1 is the nearest neighbor C atoms of vacancy defects. $E_f = (E_{total} - mE_C - nE_F)/n_{tot}$, where E_C and E_F are the energy of C and F atom obtained from diamond and F_2, respectively. The m and n represent the numbers of the C and F atoms.

	d_{C_1-C}(Å)	d_{C_1-F}(Å)	φ_{C-C_1-C}(°)	a(Å)	b(Å)	θ(°)	E_f(eV)
fluorographene	1.575	1.384	110.807	13.015	13.525	90.00	−0.862
V_F-fluorographene	1.518	1.412	113.828	12.933	13.442	90.00	−0.840
V_{sCF}-fluorographene	1.52	1.342	109.363	13.035	13.497	90.01	−0.828
V_{dCF}-fluorographene	1.523	1.361	107.185	12.931	13.254	88.47	−0.823

The formation energies of the fluorographene with vacancy defects are shown in Table 1. Even though the energies of vacancy configurations are slightly larger than that of fluorographene, the small deviations (less than 40 meV/atom) suggest that V_F-, V_{sCF}-, and V_{dCF}-fluorographene could be stabilized at nonequilibrium conditions. We performed the ab initio molecular dynamics (AIMD) simulation to verify the thermodynamic stability of fluorographene with vacancy defects at room temperature (300 K). The results are shown in Figure 2. As the variations in the total energies are within 0.15 eV/atom and the atomic structures maintain well during AIMD simulation for 10 ps, V_F-, V_{sCF}-, and V_{dCF}-fluorographene are predicted to be thermodynamically stable at room temperature.

By absorbing the F atom, the depletion of the local π bond causes charge transfer in fluorographene. Since F atom possesses a higher electronegativity than C atom, electrons transfer from the C atom to its connected F atom, indicating that C–F is a polar covalent bond. The calculated charge of the C atom and F atom, obtained by the Hirshfeld-based method [9], are +0.48, −0.48, respectively. Sounding F atom vacancy, C_0 atom remains ~4 by maintaining its unpair electron instead of reducing its electron passes to F atom, while the charge sharing of C_1–F bonds adjacent to the vacancy has some little deviations. The charge sharing of the C–F bond is closely related to the third-order nonlinear optical response [35]. The Bader charge of nearest C–F bonds in V_{sCF}- and V_{dCF}-fluorographene also has been investigated and it is convinced that the charge transfer scheme will be affected by inducing vacancy. This result is in agreement with the change of bond strength shown in Table 1.

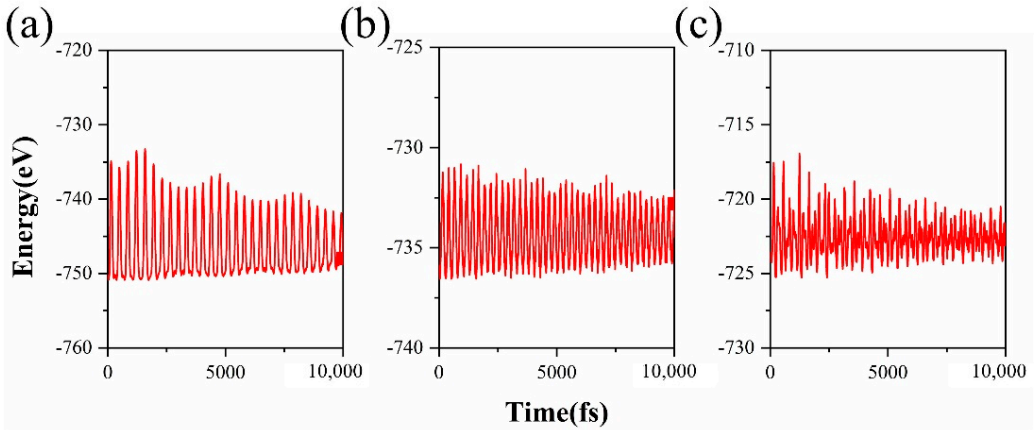

Figure 2. Variation of the total energy of (**a**) V_F-fluorographene, (**b**) V_{sCF}-fluorographene, and (**c**) V_{dCF}-fluorographene during the AIMD simulation at room temperature. The inset pictures are the atomic configurations after 10 ps.

To figure out whether vacancy can induce magnetic moment in fluorographene, we analyzed the spin density of defects structures and found that both V_F- and V_{sCF}-fluorographene are magnetic and hold 1μ_B magnetic moment, whereas V_{dCF}-fluorographene is nonmagnetic. This is consistent with the reports that only fluorinated graphene with uneven F atoms in the double sides is magnetic and can be explained by Lieb's theorem [36]. Figure 3 demonstrates the spin densities of V_F- and V_{sCF}-fluorographene. It is obvious that the magnetic moment of V_F-fluorographene mostly comes from the C_0 atom (0.72 μ_B) nearest to F vacancy, while that of V_{sCF}-fluorographene is mainly provided by C_1 atoms (0.48 μ_B, 0.49 μ_B, and -0.29 μ_B) next to the C–F vacancy. The discrepancy can be explained by the asymmetry structure as a consequence of vacancy defects. Furthermore, the three F atoms adjacent to C_1 atoms have nonnegligible contributions: 0.06 μ_B each F aligned ferromagnetically for V_F-fluorographene, (0.09 μ_B, 0.09 μ_B, -0.06 μ_B) for V_{sCF}-fluorographene.

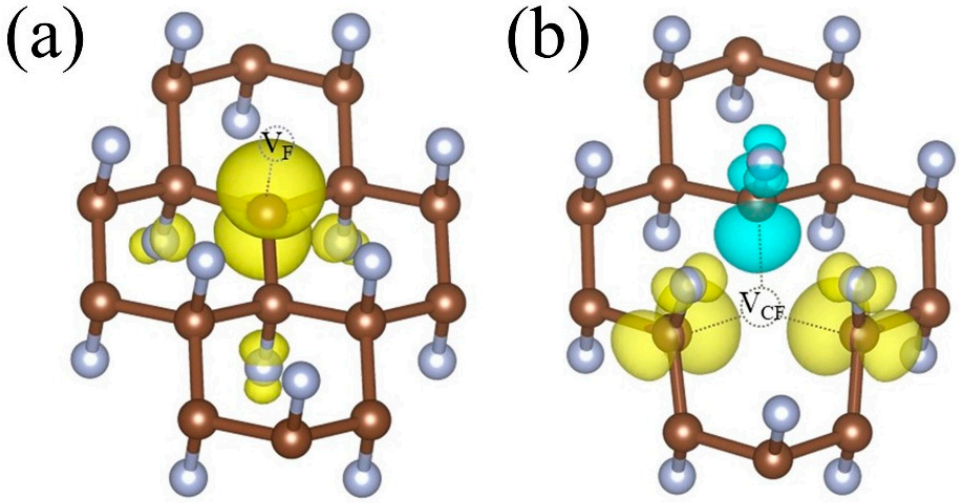

Figure 3. The spin-charge densities $n_\uparrow(r) - n_\downarrow(r)$ in (**a**) V_F-fluorographene and (**b**) V_{sCF}-fluorographene. Yellow and blue colors represent spin-up and spin-down isosurface, respectively.

The electronic properties of fluorographene and fluorographene with vacancy defects are investigated to further understand the origin of magnetism. The results are shown in Figure 4. It is revealed that fluorographene is an insulator with a bandgap of 3.09 eV, which is in good agreement with early reports (3.10 eV) [23], and V_{dCF}-fluorographene has a 3.21 eV bandgap. Both fluorographene and V_{dCF}-fluorographene have no spin splitting

(see Figure S1 in Supplementary Materials). With uneven F atoms in the double sides induced by a single F vacancy defect, midgap states appear and V_F-fluorographene is a semiconductor with a direct bandgap of 1.48 eV. The bandgap is tuned by the arise of the spin splitting. The flatness of the midgap band means that electrons are strongly localized and the localizations mainly come from p_z orbital of both C and F atoms, conforming to the characteristics of defects states. This defect level is caused by spin-down states only. Different from V_F-fluorographene, in V_{sCF}-fluorographene, the valence band maximum (VBM) and conduction band minimum (CBM) are mainly contributed by p_x and p_y orbitals of spin-up states. The bandgap decrease to 0.61 eV and V_{sCF}-fluorographene is a semiconductor with a direct bandgap. For both V_F and V_{sCF}-fluorographene, because of the exchange splitting of the defect states, the p orbital of C and F atoms is hybridized and produces exchange split bonding and antibonding states which are the origin of the induced magnetic moment near vacancy.

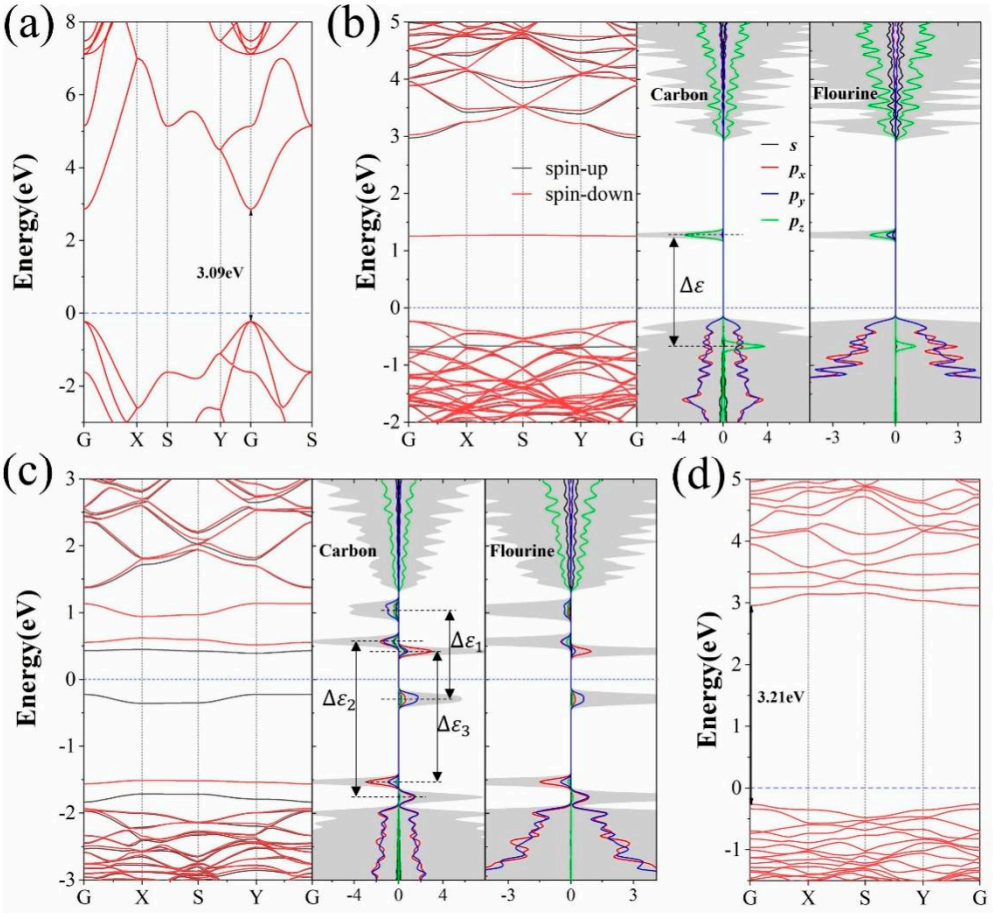

Figure 4. The band structure of (**a**) fluorographene (**b**) V_F-fluorographene (**c**) V_{sCF}-fluorographene (**d**) V_{dCF}-fluorographene. For the magnetic structures, the PDOS is shown; the black line represents the spin-up and the red line represents the spin-down; in PDOS, the black, red, blue, and green represent the s, p_x, p_y, p_z orbital of C and F, respectively. The shadow represents the total density of states and the light blue dot represents the fermi-level. $\Delta\varepsilon = \varepsilon_\uparrow - \varepsilon_\downarrow$, defined as the difference between spin-up and spin-down, is the exchange splitting energy.

Considering strain is an inevitable factor during fabrication, we further examined the strain dependence of bandgap and exchange-splitting of V_{sCF}-fluorographene. The results are shown in Figure 5. By applying strain from −0.02 to 0.02 in zigzag direction, the bandgap of V_{sCF}-fluorographene shows a linear increase from 0.51 eV to 0.78 eV. It should be noted that the position of the VBM changes infinitesimally, while the CBM changes greatly. The strain dependences of exchange-splitting are shown in Figure 5b.

It is worth mentioning that the defect states related to $\Delta\varepsilon_1$, which is mostly contributed from p_y orbitals, has a significant increase with applied strain, while that of $\Delta\varepsilon_2$ and $\Delta\varepsilon_3$ change slightly. The changes of exchange-splitting eventually tune the bandgap of V_{sCF}-fluorographene. In contrast to the bandgap, the magnetic moment of V_{sCF}-fluorographene remain $1\mu_B$ magnetic moment and show no obvious change with the uniaxial strain applied in the zigzag direction (see Table S1).

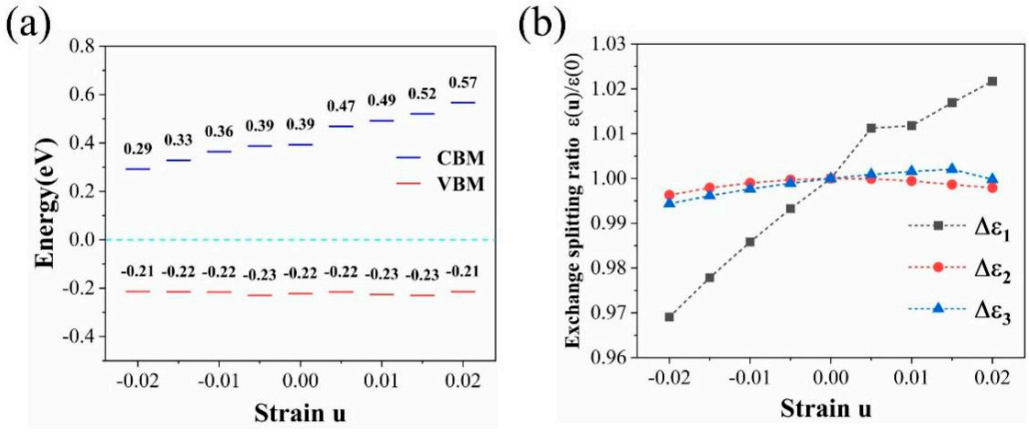

Figure 5. (**a**) Bandgap and (**b**) the exchange-splitting for V_{sCF}-fluorographene with the uniaxial strain applied in zigzag direction.

3. Method

Density functional theory (DFT) calculations are completed using the Vienna ab initio simulation package (VASP). The projector augmented wave (PAW) method and generalized gradient approximation (GGA) are performed to describe the core valence interaction and exchange-correlation [37–39]. A grid of $5 \times 5 \times 1$ kpoints generated by Monkhorst–Packscheme method [40] is used for the defect fluorographene and the cutoff energy is set as 500 eV to verify the accuracy of energy convergence. All structures are relaxed to maximum atomic forces allowance of 1×10^{-2} eV/Å and total threshold energy of 1×10^{-7} eV. Spin polarization is considered in all of the calculations by setting ISPIN = 2, and the non-collinear version of VASP is used to complete the magnetic calculation. The thickness of the vacuum layer between the monolayers is set as 15 Å to avoid the spurious interlayer interaction in the out-of-plane direction.

4. Conclusions

In summary, we studied the magnetic and electronic properties of fluorographene with three types of vacancy defects by using first-principle calculations. Our results indicate that all the three structures: V_F-, V_{sCF}-, V_{dCF}-fluorographene are stable at room temperature. Due to the uneven F atoms in the double sides caused by defects, V_F-, V_{sCF}-fluorographene has been proved to be magnetic and possesses $1\mu_B$ magnetic moments. The magnetic moment is mainly contributed by the adjacent C atoms of vacancy defects. We also investigated the strain dependence of V_{dCF}-fluorographene, and it is found that the bandgap, as well as exchange-splitting energy, can be tuned by applied strain, especially the position of the valence band. The study of fluorographene paves the way for fabricating and analyzing fluorographene-based devices.

Supplementary Materials: The following are available online, Figure S1: The band structures and DOS of fluorographene and VdCF-fluorographene, Table S1: Magnetic moment of VsCF-fluorographene with the uniaxial strain [23].

Author Contributions: Conceptualization, D.L. (Daozhi Li); methodology, D.L. (Daozhi Li); software, D.L. (Daozhi Li); validation, D.L. (Daozhi Li), X.M. and H.C.; formal analysis, X.M.; investigation, D.L.; resources, X.M. and H.C.; data curation, D.L. (Daozhi Li); writing—original draft preparation,

D.L. (Daozhi Li); writing—review and editing, X.M. and D.L. (Daozhi Li); visualization, D.L.(Daozhi Li); supervision, H.C.; project administration, D.L. (Dechun Li) and S.Z.; funding acquisition, Y.L. and D.L. (Dechun Li). All authors have read and agreed to the published version of the manuscript.

Funding: This research was funded by National Natural Science Foundation of China, grant number 12004213,12174223, 21872084.

Institutional Review Board Statement: Not applicable.

Informed Consent Statement: Not applicable.

Data Availability Statement: The data presented in this study are available on request from the corresponding author. The data are not publicly available due to ensure the security of data.

Acknowledgments: This work is supported by the National Natural Science Foundation of China (12004213, 12174223, 21872084).

Conflicts of Interest: The authors declare that they have no known competing financial interests or personal relationships that could have appeared to influence the work reported in this paper.

Sample Availability: Samples of the compounds fluorographene are available from the authors.

References

1. Novoselov, K.S.; Geim, A.K.; Morozov, S.V.; Jiang, D.; Zhang, Y.; Dubonos, S.V.; Grigorieva, I.V.; Firsov, A.A.J.S. Electric field effect in atomically thin carbon films. *Science* **2004**, *306*, 666–669. [CrossRef]
2. Lee, C.; Wei, X.; Kysar, J.W.; Hone, J. Measurement of the elastic properties and intrinsic strength of monolayer graphene. *Science* **2008**, *321*, 385–388. [CrossRef] [PubMed]
3. Wang, J.; Hernandez, Y.; Lotya, M.; Coleman, J.N.; Blau, W.J. Broadband Nonlinear Optical Response of Graphene Dispersions. *Adv. Mater.* **2009**, *21*, 2430–2435. [CrossRef]
4. Popinciuc, M.; Józsa, C.; Zomer, P.J.; Tombros, N.; Veligura, A.; Jonkman, H.T.; van Wees, B.J. Electronic spin transport in graphene field-effect transistors. *Phys. Rev. B* **2009**, *80*, 214427. [CrossRef]
5. Avsar, A.; Ochoa, H.; Guinea, F.; Özyilmaz, B.; van Wees, B.J.; Vera-Marun, I.J. Colloquium: Spintronics in graphene and other two-dimensional materials. *Rev. Mod. Phys.* **2020**, *92*, 021003. [CrossRef]
6. Wang, R.; Ren, X.G.; Yan, Z.; Jiang, L.J.; Wei, E.; Shan, G.C. Graphene based functional devices: A short review. *Front. Phys.* **2019**, *14*, 13603. [CrossRef]
7. Bonaccorso, F.; Sun, Z.; Hasan, T.; Ferrari, A. Graphene photonics and optoelectronics. *Nat. Photonics* **2010**, *4*, 611–622. [CrossRef]
8. Yu, X.; Cheng, H.; Zhang, M.; Zhao, Y.; Qu, L.; Shi, G. Graphene-based smart materials. *Nat. Rev. Mater.* **2017**, *2*, 17046. [CrossRef]
9. Henkelman, G.; Arnaldsson, A.; Jónsson, H. A fast and robust algorithm for Bader decomposition of charge density. *Comput. Mater. Sci.* **2006**, *36*, 354–360. [CrossRef]
10. Solís-Fernández, P.; Bissett, M.; Ago, H. Synthesis, structure and applications of graphene-based 2D heterostructures. *Chem. Soc. Rev.* **2017**, *46*, 4572–4613. [CrossRef]
11. Kuila, T.; Bose, S.; Mishra, A.K.; Khanra, P.; Kim, N.H.; Lee, J.H. Chemical functionalization of graphene and its applications. *Prog. Mater. Sci.* **2012**, *57*, 1061–1105. [CrossRef]
12. Bottari, G.; Herranz, M.Á.; Wibmer, L.; Volland, M.; Rodríguez-Pérez, L.; Guldi, D.M.; Hirsch, A.; Martín, N.; D'Souza, F.; Torres, T. Chemical functionalization and characterization of graphene-based materials. *Chem. Soc. Rev.* **2017**, *46*, 4464–4500. [CrossRef] [PubMed]
13. Todd, K.; Chou, H.T.; Amasha, S.; Goldhaber-Gordon, D. Quantum Dot Behavior in Graphene Nanoconstrictions. *Nano Lett.* **2009**, *9*, 416–421. [CrossRef] [PubMed]
14. Karlický, F.; Kumara Ramanatha Datta, K.; Otyepka, M.; Zbořil, R. Halogenated Graphenes: Rapidly Growing Family of Graphene Derivatives. *ACS Nano* **2013**, *7*, 6434–6464. [CrossRef] [PubMed]
15. Compton, O.C.; Nguyen, S.T. Graphene Oxide, Highly Reduced Graphene Oxide, and Graphene: Versatile Building Blocks for Carbon-Based Materials. *Small* **2010**, *6*, 711–723. [CrossRef]
16. Yao, Z.; Nie, H.; Yang, Z.; Zhou, X.; Liu, Z.; Huang, S. Catalyst-free synthesis of iodine-doped graphenevia a facile thermal annealing process and its use for electrocatalytic oxygen reduction in an alkaline medium. *Chem. Commun.* **2012**, *48*, 1027–1029. [CrossRef]
17. Hong, X.; Zou, K.; Wang, B.; Cheng, S.H.; Zhu, J. Evidence for Spin-Flip Scattering and Local Moments in Dilute Fluorinated Graphene. *Phys. Rev. Lett.* **2012**, *108*, 226602. [CrossRef]
18. Jiang, L.; Fu, W.; Birdja, Y.Y.; Koper, M.T.M.; Schneider, G.F. Quantum and electrochemical interplays in hydrogenated graphene. *Nat. Commun.* **2018**, *9*, 793. [CrossRef]
19. Li, B.; Zhou, L.; Wu, D.; Peng, H.; Yan, K.; Zhou, Y.; Liu, Z. Photochemical Chlorination of Graphene. *ACS Nano* **2011**, *5*, 5957–5961. [CrossRef]

20. Olanrele, S.O.; Lian, Z.; Si, C.; Chen, S.; Li, B. Tuning of interactions between cathode and lithium polysulfide in Li-S battery by rational halogenation. *J. Energy Chem.* **2020**, *49*, 147–152. [CrossRef]
21. Eng, A.Y.S.; Sofer, Z.; Bouša, D.; Sedmidubský, D.; Huber, Š.; Pumera, M. Near-Stoichiometric Bulk Graphane from Halogenated Graphenes (X = Cl/Br/I) by the Birch Reduction for High Density Energy Storage. *Adv. Funct. Mater.* **2017**, *27*, 1605797. [CrossRef]
22. Tran, N.T.T.; Nguyen, D.K.; Glukhova, O.E.; Lin, M.F. Coverage-dependent essential properties of halogenated graphene: A DFT study. *Sci. Rep.* **2017**, *7*, 17858. [CrossRef]
23. Feng, W.; Long, P.; Feng, Y.; Li, Y. Two-Dimensional Fluorinated Graphene: Synthesis, Structures, Properties and Applications. *Adv. Sci.* **2016**, *3*, 1500413. [CrossRef] [PubMed]
24. Urbanová, V.; Karlický, F.; Matěj, A.; Šembera, F.; Janoušek, Z.; Perman, J.A.; Ranc, V.; Čépe, K.; Michl, J.; Otyepka, M.; et al. Fluorinated graphenes as advanced biosensors—Effect of fluorine coverage on electron transfer properties and adsorption of biomolecules. *Nanoscale* **2016**, *8*, 12134–12142. [CrossRef]
25. Liu, H.Y.; Hou, Z.F.; Hu, C.H.; Yang, Y.; Zhu, Z.Z. Electronic and Magnetic Properties of Fluorinated Graphene with Different Coverage of Fluorine. *J. Phys. Chem. C* **2012**, *116*, 18193–18201. [CrossRef]
26. Nair, R.R.; Ren, W.; Jalil, R.; Riaz, I.; Kravets, V.G.; Britnell, L.; Blake, P.; Schedin, F.; Mayorov, A.S.; Yuan, S.; et al. Fluorographene: A Two-Dimensional Counterpart of Teflon. *Small* **2010**, *6*, 2877–2884. [CrossRef]
27. Cheng, S.H.; Zou, K.; Okino, F.; Gutierrez, H.R.; Gupta, A.; Shen, N.; Eklund, P.C.; Sofo, J.O.; Zhu, J. Reversible fluorination of graphene: Evidence of a two-dimensional wide bandgap semiconductor. *Phys. Rev. B* **2010**, *81*, 205435. [CrossRef]
28. Jeon, K.J.; Lee, Z.; Pollak, E.; Moreschini, L.; Bostwick, A.; Park, C.M.; Mendelsberg, R.; Radmilovic, V.; Kostecki, R.; Richardson, T.J. Fluorographene: A Wide Bandgap Semiconductor with Ultraviolet Luminescence. *ACS Nano* **2011**, *5*, 1042–1046. [CrossRef] [PubMed]
29. Bon, S.B.; Valentini, L.; Verdejo, R.; Fierro, J.G.; Peponi, L.; Lopez-Manchado, M.A.; Kenny, J.M. Plasma Fluorination of Chemically Derived Graphene Sheets and Subsequent Modification With Butylamine. *Chem. Mater.* **2009**, *21*, 3433–3438. [CrossRef]
30. Herraiz, M.; Dubois, M.; Batisse, N.; Hajjar-Garreau, S.; Simon, L. Large-scale synthesis of fluorinated graphene by rapid thermal exfoliation of highly fluorinated graphite. *Dalton Trans.* **2018**, *47*, 4596–4606. [CrossRef]
31. Banhart, F.; Kotakoski, J.; Krasheninnikov, A.V. Structural defects in graphene. *ACS Nano* **2011**, *5*, 26–41. [CrossRef]
32. Kanoun, M.B. Vacancy defects- and strain-tunable electronic structures and magnetism in two-dimensional MoTe 2: Insight from First-Principles Calculations. *Surf. Interfaces* **2021**, *27*, 101442. [CrossRef]
33. Ye, J.; An, Y.; Yan, H.; Liu, J. Defects and strain engineering the electronic structure and magnetic properties of monolayer WSe2 for 2D spintronic device. *Appl. Surf. Sci.* **2019**, *497*, 143788. [CrossRef]
34. Şahin, H.; Topsakal, M.; Ciraci, S. Structures of fluorinated graphene and their signatures. *Phys. Rev. B* **2011**, *83*, 115432. [CrossRef]
35. Papadakis, I.; Stathis, A.; Bourlinos, A.B.; Couris, S. Diethylamino-fluorographene: A 2D material with broadband and efficient optical limiting performance (from 500 to 1800 nm) with very large nonlinear optical response. *Nano Sel.* **2020**, *1*, 395–404. [CrossRef]
36. Zheng, Y.; Wan, X.; Tang, N.; Feng, Q.; Liu, F.; Du, Y. Magnetic properties of double-side partially fluorinated graphene from first principles calculations. *Carbon* **2015**, *89*, 300–307. [CrossRef]
37. Perdew, J.P.; Burke, K.; Ernzerhof, M. Generalized gradient approximation made simple. *Phys. Rev. Lett.* **1996**, *77*, 3865. [CrossRef] [PubMed]
38. Kresse, G.; Furthmüller, J. Efficient iterative schemes for ab initio total-energy calculations using a plane-wave basis set. *Phys. Rev. B* **1996**, *54*, 11169. [CrossRef]
39. Kresse, G.; Joubert, D. From ultrasoft pseudopotentials to the projector augmented-wave method. *Phys. Rev. B* **1999**, *59*, 1758–1775. [CrossRef]
40. Monkhorst, H.J.; Pack, J.D. Special points for Brillouin-zone integrations. *Phys. Rev. B Condens. Matter* **1976**, *13*, 5188–5192. [CrossRef]